Biogeosciences

Open Access

The effects of river inflow and retention time on the spatial heterogeneity of chlorophyll and water–air CO_2 fluxes in a tropical hydropower reservoir

F. S. Pacheco[1], M. C. S. Soares[2], A. T. Assireu[3], M. P. Curtarelli[4], F. Roland[2], G. Abril[5], J. L. Stech[4], P. C. Alvalá[1], and J. P. Ometto[1]

[1]Earth System Science Center, National Institute for Space Research, São José dos Campos, 12227–010, São Paulo, Brazil
[2]Laboratory of Aquatic Ecology, Federal University of Juiz de Fora, Juiz de Fora, 36036–900, Minas Gerais, Brazil
[3]Institute of Natural Resources, Federal University of Itajubá, Itajubá, 37500–903, Minas Gerais, Brazil
[4]Remote Sense Division, National Institute for Space Research, São José dos Campos, 12227–010, São Paulo, Brazil
[5]Laboratoire Environnements et Paléoenvironnements Océaniques et Continentaux (EPOC), CNRS, Université Bordeaux 1, Avenue des Facultés, 33405 Talence, France

Correspondence to: F. S. Pacheco (felipe.pacheco@inpe.br)

Abstract. Abundant research has been devoted to understanding the complexity of the biogeochemical and physical processes that are responsible for greenhouse gas (GHG) emissions from hydropower reservoirs. These systems may have spatially complex and heterogeneous GHG emissions due to flooded biomass, river inflows, primary production and dam operation. In this study, we investigated the relationships between the water–air CO_2 fluxes and the phytoplanktonic biomass in the Funil Reservoir, which is an old, stratified tropical reservoir that exhibits intense phytoplankton blooms and a low partial pressure of CO_2 (pCO_2). Our results indicated that the seasonal and spatial variability of chlorophyll concentrations (Chl) and pCO_2 in the Funil Reservoir are related more to changes in the river inflow over the year than to environmental factors such as air temperature and solar radiation. Field data and hydrodynamic simulations revealed that river inflow contributes to increased heterogeneity during the dry season due to variations in the reservoir retention time and river temperature. Contradictory conclusions could be drawn if only temporal data collected near the dam were considered without spatial data to represent CO_2 fluxes throughout the reservoir. During periods of high retention, the average CO_2 fluxes were $10.3\ \mathrm{mmol\,m^{-2}\,d^{-1}}$ based on temporal data near the dam versus $-7.2\ \mathrm{mmol\,m^{-2}\,d^{-1}}$ with spatial data from along the reservoir surface. In this case, the use of solely temporal data to calculate CO_2 fluxes results in the reservoir acting as a CO_2 source rather than a sink. This finding suggests that the lack of spatial data in reservoir C budget calculations can affect regional and global estimates. Our results support the idea that the Funil Reservoir is a dynamic system where the hydrodynamics represented by changes in the river inflow and retention time are potentially a more important force driving both the Chl and pCO_2 spatial variability than the in-system ecological factors.

1 Introduction

Over the last two decades, hydropower reservoirs have been identified as potentially important sources of greenhouse gas (GHG) emissions (St Louis et al., 2000; Rosa et al., 2004; Demarty et al., 2011). In tropical regions, high temperatures and forest flooding have intensified GHG emissions (Abril et al., 2005; Fearnside and Pueyo, 2012). However, emissions are larger in tropical Amazonian (Abril et al., 2013) than in tropical non-Amazonian reservoirs (Ometto et al., 2011) and are larger in younger than in older reservoirs (Barros et al., 2011). Large hydroelectric reservoirs, particularly those created by impounded rivers, are morphometrically complex
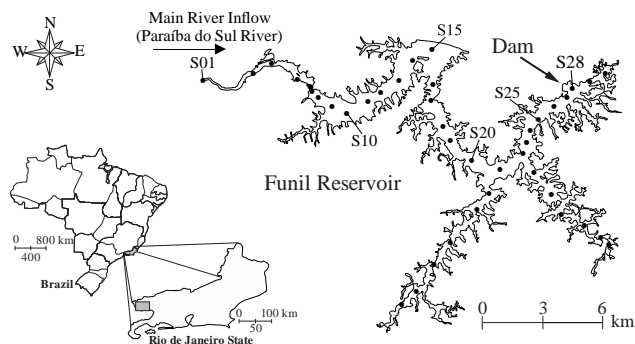
Figure 1. Map of the Funil Reservoir showing the geographic location and sampling stations.

and spatially heterogeneous (Roland et al., 2010; Teodoru et al., 2011; Zhao et al., 2013). Different regions of the reservoir may have different CO_2 dynamics because of flooded biomass, river input of organic matter, primary production and dam operations. Furthermore, both heterotrophic and autotrophic activities influence the CO_2 concentrations along reservoirs located in subtropical (Di Siervi et al., 1995), tropical (Roland et al., 2010; Kemenes et al., 2011) and temperate areas (Richardot et al., 2000; Lauster et al., 2006; Finlay et al., 2009; Halbedel and Koschorreck, 2013).

As sedimentation and light availability increase along a reservoir, the biomass of the primary producers may increase. Phytoplankton is distributed in patches along the reservoir due to differences in the nutrient distribution, light availability and stratification (Serra et al., 2007). Additionally, hydrodynamics factors, such as retention time and river inflow, may influence the phytoplankton communities and their growth (Vidal et al., 2012; Soares et al., 2008). Intense phytoplankton primary production has been identified as the main regulator of carbon (C) budgets in temperate eutrophic lakes (Finlay et al., 2010; Pacheco et al., 2014); however, the impact of these communities on tropical hydropower reservoirs is still unclear.

River inflows may affect the biogeochemical patterns in river valley reservoirs (Kennedy, 1999). Density differences of incoming stream and lake water, the stream and lake hydraulics, the strength of stratification and mixing patterns are all features that control how river water will flow when it reaches the reservoir (Fischer and Smith, 1983; Fischer et al., 1979). As a result of density differences between river and lake water, a river enters a lake and can flow large distances as a gravity-driven density current (Ford, 1990; Martin and McCutcheon, 1998). The interactions of large nutrient loads injected by rivers and the dynamics of river inflow can determine the spatial heterogeneity of phytoplankton distribution (Vidal et al., 2012). Consequently, the river inflow may affect primary production along a river/dam axis in hydropower reservoirs that are strongly influenced by rivers with high nutrient levels.

In this study, we investigated the relationships between phytoplanktonic biomass and water–air CO_2 fluxes in an old, stratified tropical reservoir (Funil, state of Rio de Janeiro, Brazil) where intense phytoplankton blooms and low pCO$_2$ are observed in the water. We combined fieldwork and modeling to analyze the impact of meteorological and hydrological factors on the spatial and temporal dynamics of phytoplankton and the intensity of CO_2 fluxes. We demonstrate the effect of river inflow on the heterogeneity of pCO$_2$ and Chl in the Funil Reservoir. We also compare temporal data of the pCO$_2$ collected near the dam with a high density of spatial data. Our hypothesis is that the seasonal and spatial variability of pCO$_2$ and Chl in the Funil Reservoir is related more to the river inflow and retention time than to external environmental factors such as air temperature and solar radiation. We highlight that very different conclusions can be drawn about carbon cycling in reservoirs if the spatial heterogeneity is not adequately considered.

2 Materials and methods

2.1 Study site

The Funil Reservoir is an old impoundment constructed at the end of the 1960s that is located on the Paraíba do Sul River, in the southern part of the state of Rio de Janeiro, Brazil ($22°30'$ S, $44°45'$ W; Fig. 1). The site is 440 m above sea level, with wet-warm summers and dry-cold winters. The Funil Reservoir mainly functions for energy production, but the reservoir is also used for irrigation and recreation. It has a surface area of $40\,km^2$, a mean and maximum depth of 22 and 74 m, respectively, and a total volume of $890 \times 10^6\,m^3$. The maximum and minimum reservoir water level occurs at the end of the rainy season (April) and dry season (October), respectively. From October 2011 to September 2012, the difference between the minimum and maximum water level was 15.6 m and the average retention time was 32 days.

The Funil Reservoir has a catchment area of $12\,800\,km^2$ that is one of the most highly industrialized regions in Brazil. There are approximately 2 million people living inside the catchment area and 39 cities that depend on the Paraíba do Sul River for their water supply. These cities represent 2 % of Brazil's gross domestic product (GDP) (IBGE, 2010). In this area, 46 % of the sewage is untreated (AGEVAP, 2011), and the Paraíba do Sul River receives a large portion of the sewage from one of the most populated regions in Brazil (20–50 inhabitants per square kilometer; IBGE, 2010). Consequently, the river exerts a large influence on the reservoir's water quality, and the reservoir has experienced tragic eutrophication in recent decades, resulting in frequent and intense cyanobacterial blooms (Klapper, 1998; Branco et al., 2002; Rocha et al., 2002). The river inflow is affected by the water supply and the operation of upstream dams. In general, the Funil Reservoir is a turbid, eutrophic system, with high
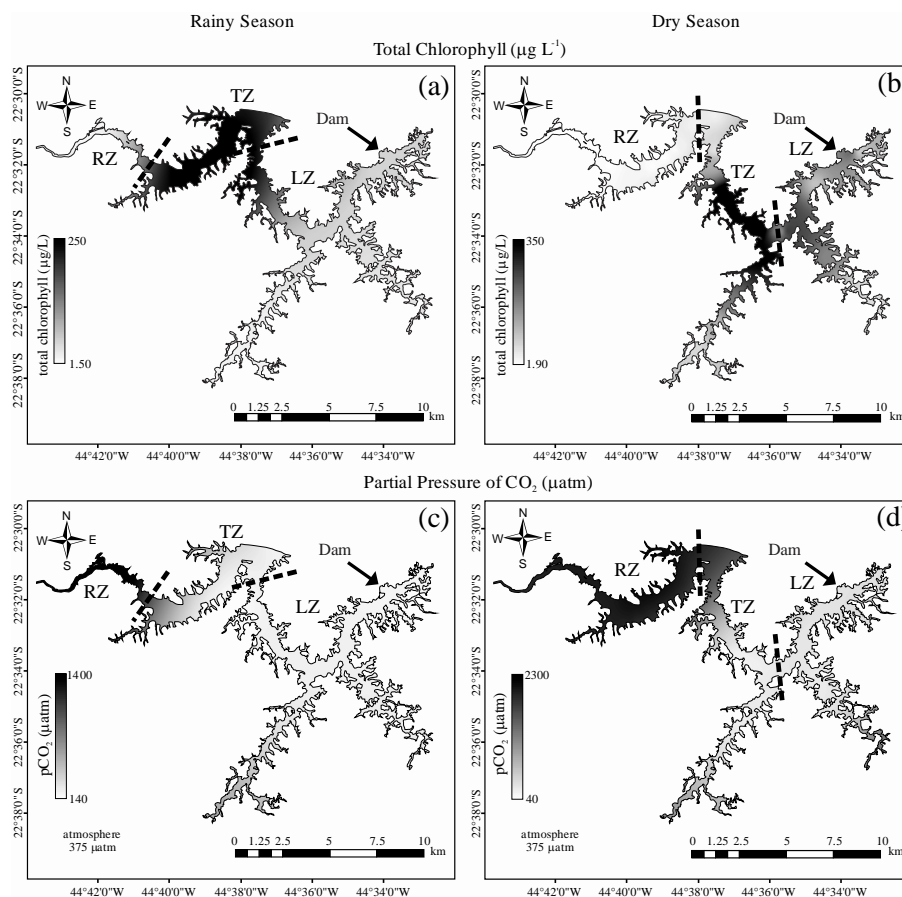
Figure 2. Map of $p\mathrm{CO_2}$ and Chl as expressed by a color gradient obtained from interpolation of measured data using ordinary kriging statistics. The root-mean-square error (RMSE) of the kriging prediction, calculated by comparing observed and calculated values, was 90 µatm and 15 µg L^{-1} for $p\mathrm{CO_2}$ and Chl, respectively. Lighter gray represents low Chl **(a, b)** and low $p\mathrm{CO_2}$ **(c, d)**. RZ: riverine zone; TZ: transition zone; LZ: lacustrine zone.

levels of phytoplankton (cyanobacteria) biomass (Soares et al., 2012; Rangel et al., 2012).

2.2 Field sampling

Spatial data: we considered 42 stations in the Funil Reservoir (28 were located along the main body of the reservoir, Fig. 1) for the spatial analyses. Water samples to determine Chl and $p\mathrm{CO_2}$ were obtained between 9:00 and 12:00 local time (LT: UTC/GMT -3 h) on 1 March 2012 (at the end of the rainy season, at high water levels) and on 20 September 2012 (at the end of the dry season, at low water levels). Samples were taken from the surface (0.3 m) on the same day to limit the effect of diurnal variations on the results. We measured Chl using a compact version of PHYTO-PAM (Heinz Walz GmbH, PHYTO-ED, Effelrich, Germany). The $p\mathrm{CO_2}$ data were determined using a water–air equilibration method. In a marble-type equilibrator (Abril et al., 2014, 2006), the water was pumped directly from the lake and flowed from the top to the bottom (0.8 L min^{-1}), whereas a constant volume of air (0.4 L min^{-1}) flowed from the bottom to the top. The

large gas exchange surface area promoted by contact with the marbles accelerated the $p\mathrm{CO_2}$ water–air equilibrium. The air pump conducted the air from the top of the equilibrator through a drying tube containing a desiccant (Drierite), then to an infrared gas analyzer (IRGA; LI-840, LICOR, Lincoln, NE, USA) and back to the bottom of the equilibrator (closed air circuit; Abril et al., 2006). For each station, the lake water and air were pumped through the system for 2 min before the $p\mathrm{CO_2}$ from the IRGA stabilized to a constant value.

Color maps were created to represent the spatial distribution of Chl and $p\mathrm{CO_2}$ (Fig. 2). We used a variogram analysis to describe the spatial correlation among the samples and to spatially interpolate with kriging (Bailey and Gatrell, 1995). The empirical variograms were fitted to different mathematical models using the Akaike's information criterion (AIC; Akaike, 1974) to evaluate the best fit. The best variogram model was used for interpolation with ordinary kriging. We used the Spring software (National Institute for Space Research, São José dos Campos, SP, Brazil; Câmara et al.,

1996) version 5.1.8 to conduct a spatial analysis and to produce in situ pCO_2 and Chl maps.

In this study, we used Chl as a parameter to separate the reservoir into three zones. The riverine zone is characterized by low Chl ($< 5\,\mu g\,L^{-1}$). The transition zone begins where the Chl starts to increase ($> 5\,\mu g\,L^{-1}$) and ends when the Chl decreases to levels close to the Chl in the lacustrine zone ($< 60\,\mu g\,L^{-1}$). Finally, the lacustrine zone is characterized by intermediate Chl levels (> 5 and $< 60\,\mu g\,L^{-1}$); however, peaks of Chl were observed in some parts of the lacustrine zone. We estimated the size of each zone (riverine, transition, lacustrine) of the reservoir during the dry and rainy seasons using the results from the spatial interpolation of the Chl data. After the interpolation, we used a pixel classification method to determine the boundaries of each zone (class). We checked the boundary locations with observed data. Finally, we determined the area by multiplying the number of pixels of each class by the area of each pixel. The boundary of each zone is represented by dashed lines on the maps (Fig. 2).

Time series data: the temporal data were collected at a single station (S28) near the dam (Fig. 1). Wind speed and direction, solar radiation, pH, dissolved oxygen (DO), air temperature and temperature profiles (2, 5, 20 and 40 m depth) were collected hourly and transmitted by satellite in quasi-real time by the Integrated System for Environmental Monitoring (SIMA). SIMA is a set of hardware and software developed for data acquisition and real-time monitoring of hydrological systems (Alcantara et al., 2013; Stevenson et al., 1993). SIMA consists of an independent system formed by an anchored buoy containing data storage systems, sensors (air temperature, wind direction and intensity, pressure, incoming and reflected radiation, and a thermistor chain), a solar panel, a battery and a transmission antenna. A sonde probe (YSI model 6600, Yellow Spring, OH, USA) was attached to the SIMA buoy to collect hourly surface data on temperature, conductivity, pH and oxygen. The sonde was calibrated every 15 days based on the YSI Environmental Operations Manual (http://www.ysi.com/ysi/support). We used data collected between 25 October 2011 and 25 October 2012 for our analyses.

Samples for alkalinity (ALK), total phosphorous (TP) and nitrogen (TN) analyses were taken monthly. ALK was determined by the titration method (APHA, 2005). For TP, the samples were oxidized by persulfate and were then analyzed as soluble reactive phosphorus. TN was determined as the sum of the organic fraction measured with the Kjedahl method and the dissolved inorganic nutrients. A laboratory analysis of TP and NP was performed based on standard spectrophotometric techniques (Wetzel and Likens, 2010).

We calculated the pCO_2 from the surface water over 1 year near the dam using the measured pH and alkalinity. The calculations included the dependence on temperature for the dissociation constants of carbonic acid (Millero et al., 2002) and the solubility of CO_2. We used the hourly data of pH and temperature and the monthly data of alkalinity collected at station S28 (Fig. 1).

2.3　CO$_2$ flux calculation

The air–water flux of CO_2 ($mmol\,m^{-2}\,d^{-1}$) was calculated according to Eq. (1). Positive values of CO_2 fluxes denote the net gas flux from the lake to the atmosphere,

$$F(CO_2) = k\alpha\Delta pCO_2, \tag{1}$$

where k is the gas transfer velocity of CO_2 (in $m\,h^{-1}$), α is the solubility coefficient of CO_2 (in $mmol\,m^{-3}\,\mu atm^{-1}$) as a function of water temperature (Weiss, 1974), and ΔpCO_2 is the air–water gradient of pCO_2 (in μatm). The atmospheric pCO_2 measured during the rainy and dry season was 375 μatm, and this atmospheric value was used for all of the flux calculations. The gas transfer velocity k was calculated from the gas transfer velocity normalized to a Schmidt number of 600 (k_{600}) that corresponds to the CO_2 at 20 °C (Eq. 2) (Jahne et al., 1987), as follows:

$$k = k_{600}\left(\frac{Sc}{600}\right)^{-0.5}, \tag{2}$$

where Sc is the Schmidt number of a given gas at a given temperature (Wanninkhof, 1992). k_{600} is the normalized gas transfer velocity calculated from the wind speed (MacIntyre et al., 2010) using different equations under cooling and heating conditions (Eqs. 3, 4). We also evaluated a wind-speed formulation by Cole and Caraco (1998) to investigate the importance of different formulation of k_{600} (Eq. 5). A more detailed description for these equations is in Staehr et al. (2012). The k_{600} was calculated in $cm\,h^{-1}$ and were converted to $m\,d^{-1}$.

$$k_{600} = 2.04\,U_{10} + 2.0 \tag{3}$$

(under cooling; MacIntyre et al., 2010),

$$k_{600} = 1.74\,U_{10} - 0.15 \tag{4}$$

(under heating; MacIntyre et al., 2010),

$$k_{600} = 2.07 + 0.21\,U_{10}^{1.7} \tag{5}$$

(Cole and Caraco, 1998),

where U_{10} is the wind speed at 10 m height. The wind speed was obtained from SIMA data at 3 m height and was calculated at 10 m height (Smith, 1985).

In the riverine zone, we considered the k_{600} as a function of wind and water currents. The contribution of the water current to the gas transfer velocity was estimated using the water current (w, $cm\,s^{-1}$) and depth (h, m) and the equations in Borges et al. (2004) (Eq. 6):

$$k_{600} = 1.719\,w^{0.5}h^{-0.5}. \tag{6}$$

2.4 Temperature profile

Temperature profiles were collected using a thermistor chain deployed at station S09 during the rainy season and station S14 during the dry season to determine the thermal structure in the transition zone. Eleven thermistors (Hobo, U22 Water Temp Pro v2, Bourne, MA, USA) were placed every 0.5 m up to 4 m and every 1 m from 5 to 7 m. We also deployed a thermistor chain at the riverine zone at station S05 with thermistors placed every 2 m. The thermistors were programmed to record the temperature every 10 min. During the rainy season, the thermistor chain was deployed on 29 February 2012 at 18:30 LT and was recovered after 40 h. In the dry season, the thermistor chain was deployed on 20 September 2012 at 11:30 LT and was recovered after 25 h.

In our analysis, the temperature was considered to be the factor controlling water density. The use of temperature is justified by the low conductivity and turbidity in the river. The turbidity values of 29 and 11 NTU that were measured during the rainy and dry seasons, respectively, would have affected density $< 5\%$ relative to temperature (Gippel, 1989).

2.5 Numerical model description and setup

Numerical simulations of lake hydrodynamics were conducted with the Estuary and Lake Computer Model (EL-COM; Hodges et al., 2000). This model solves the 3-D hydrostatic, Boussinesq, Reynolds-averaged Navier–Stokes and scalar transport equations, separating mixing of scalars and momentum from advection. The hydrodynamic algorithms that are implemented in the ELCOM use a Euler–Lagrange approach for the advection of momentum adapted from the work of Casulli and Cheng (1992), whereas the advection of scalars (i.e., tracers, conductivity and temperature) is based on the ULTIMATE QUICKEST method proposed by Leonard (1991). The thermodynamics model considers the penetrative (i.e., shortwave radiation) and non-penetrative components (i.e., longwave radiation, sensible and latent heat fluxes) (Hodges et al., 2000). The vertical mixing model uses the transport equations of turbulent kinetic energy (TKE) to compute the energy available from wind stirring and shear production for the mixing process (Spigel and Imberger, 1980). A complete description of the formulae and numerical methods used in the ELCOM was given by Hodges et al. (2000).

Hydrodynamic simulations of the Funil Reservoir were conducted under realistic forcing conditions (e.g., inflow, outflow, atmospheric temperature and radiation). These simulations were aimed at testing hypotheses about river inflows in transition zones during the rainy and dry seasons in the Funil Reservoir. The simulations started 4 days before our study period. This was necessary to let the model equilibrate beyond the initial physical conditions. The digital representation of the reservoir bathymetry (numerical domain) was defined based on the bathymetric data collected from 27 to 29

February 2012. The numerical domain was discretized in a uniform horizontal grid containing 100 m x 100 m cells. The vertical grid resolution was set to a uniform 1 m of thickness, resulting in 72 vertical layers. The water albedo was set to 0.03 (Slater, 1980), and the bottom drag coefficient was set to 0.001 (Wüest and Lorke, 2003). The attenuation coefficient for PAR was set to $0.6\,\mathrm{m}^{-1}$ based on Secchi disk measurements. Based on a previous study conducted in another tropical reservoir (Pacheco et al., 2011), a value of $5.25\,\mathrm{m}^2\,\mathrm{s}^{-1}$ was chosen for the horizontal diffusivity of temperature and for the horizontal momentum.

Because of the presence of persistent unstable atmospheric conditions over tropical reservoirs (Verburg and Antenucci, 2010), an atmospheric stability sub-model was activated during the simulation; this procedure was adequate because the meteorological sensors were placed within the atmospheric boundary layer (ABL) over the surface of the lake and the data were collected at sub-daily intervals (Imberger and Patterson, 1990). In this manner, at each model time step, the heat and momentum transfer coefficients were adjusted based on the stability of the ABL. The stability of the ABL is evaluated through the stability parameter, which was derived from the Monin–Obukhov length scale. ELCOM uses similarity functions presented in Imberger and Patterson (1990) in both stable (negative values stability parameter) and unstable conditions (positive values). The Coriolis sub-model was also activated during the simulation and the Coriolis force was then considered in the Navier–Stokes equation. This force causes the deflection of moving objects (in this case, the water currents) when they are viewed in a rotating reference frame (e.g., the Earth).

We defined two sets of boundary cells to force the inflow (Paraíba do Sul River) and outflow (the water intake at the dam). The meteorological driving forces over the free surface of the reservoir were considered uniform. The model was forced using hourly meteorological data acquired by SIMA, the daily inflow and outflow provided by Eletrobrás-Furnas, and the river temperatures extracted from thermistor chain data. To complement river inflow temperature data collected in situ, we used the Moderate Resolution Imaging Spectroradiometer (MODIS; Justice et al., 2002) level 3 land surface temperature (LST) product (named M*D11A1; see Wan, 2008, for more details) to estimate the temporal variation of temperature at the reservoir's inflow. The M*D11A1 is a standard remote-sensing-based product, generated using a split-window algorithm and seven spectral MODIS bands located in the regions of the shortwave infrared and thermal infrared bands. This algorithm is based on the differential absorption of adjacent bands in the infrared region (Wan and Dozier, 1996). The M*D11A1 product has been validated at stage 2 by a series of field campaigns conducted between 2000 and 2007 and over more locations and time periods during radiance-based validation studies. Accuracy is better than 1 °C (0.5 °C in most cases). This product is generated up to four times each day (i.e., 10:30, 13:30, 23:30 and 02:30) and

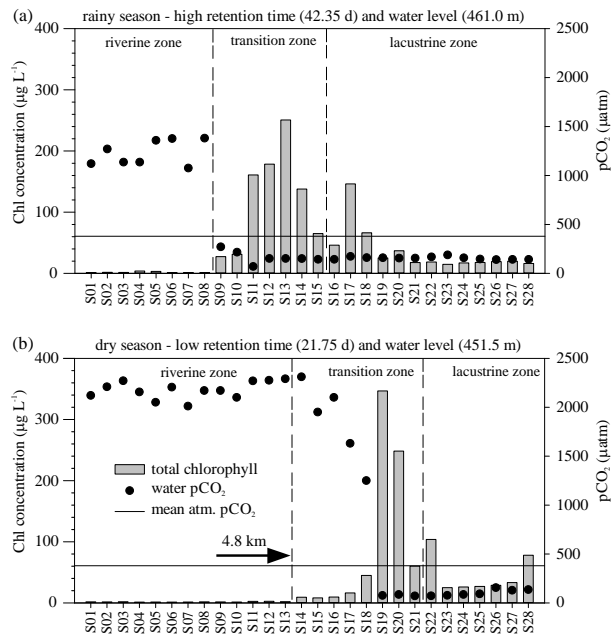**Figure 3.** Lotic–lentic gradient of pCO_2 and Chl at the 28 sampling stations in the main reservoir body during the rainy season **(a)** and dry season **(b)**. The water level was 461.0 and 451.5 m during the rainy season and dry season, respectively. Three zones can be clearly defined (riverine, transition and lacustrine zones). The arrow shows that the transition zone starts 4.8 km down-reservoir during a period of low water levels.

is delivered in a georeferenced grid with 1 km of spatial resolution in a sinusoidal projection by the National Aeronautics and Space Administration Land Processes Distributed Active Archive Center (NASA LP DAAC).

The cloud cover fraction over the Funil Reservoir was estimated using a MODIS level 2 cloud mask product (named M*D35L2; see Ackerman et al., 1998, for more details). The algorithm used to generate the M*D35L2 product employs a series of visible and infrared threshold and consistency tests to specify confidence that an unobstructed view of the Earth's surface is observed. This product is generated up to four times each day (i.e., 10:30, 13:30, 23:30 and 02:30) and is delivered in a georeferenced grid with 1 km of spatial resolution in a sinusoidal projection.

The MODIS products were acquired online (http://reverb.echo.nasa.gov/reverb/) and were preprocessed using the MODIS Reprojection Tool (available at https://lpdaac.usgs.gov). The data were first resampled to a 100 m spatial resolution (compatible with the bathymetric grid). Next, they were re-projected into the universal transverse mercator (UTM) coordinate system (zone 23 south) with the World Geodetic System (WGS-84) datum as reference; then, they were converted into a raster image. Finally, MATLAB® routines were used to calculate the river inflow temperature and cloud cover fraction time series. The river inflow temperature (°C) time series was computed

using the preprocessed M*D11A1 data by extracting the temperature values from the pixel located within the Paraíba do Sul River channel near the Funil Reservoir entrance. The cloud cover fraction (dimensionless) time series was obtained using the preprocessed M*D35L2 data by computing the ratio between the cloudy pixels and the total pixels covering the reservoir surface. Two periods were simulated: one to represent the rainy season (25 February 2012 to 4 March 2012) and one to represent the dry season (15 to 23 September 2012).

3 Results

3.1 Spatial variability

Based on the spatial data of Chl and pCO_2, a typical zonation pattern that is usually found in reservoirs was observed in the main sections of the Funil Reservoir (riverine, transition and lacustrine zones) (Fig. 2). Although the boundaries are influenced by many factors and are not easily determined, these regions have distinct physical, chemical and biological features. The riverine zone (RZ) has a high input of nutrients coming from terrestrial systems and human activities, but primary production is limited by high turbidity and turbulence. As the sedimentation and light availability increase along the reservoir, the biomass of the primary producers increases in the transition zone (TZ). The lacustrine zone (LZ) is characterized by nutrient limitations and reduced phytoplankton biomass (Thornton, 1990).

The Funil Reservoir was spatially heterogeneous with seasonal differences in the Chl and pCO_2 (Fig. 2). There was only high spatial variation in the main body of the reservoir, whereas the southern part was undersaturated in CO_2 during the rainy and dry seasons (Fig. 2a, b). The spatial averages of pCO_2 during the rainy and dry season were 259 ± 221 and 881 ± 900 µatm, respectively. The pCO_2 varied from 140 to 1376 µatm during the rainy season and from 43 to 2290 µatm during the dry season. Higher values of pCO_2 in the riverine zone of the reservoir and a drastic decrease in the transition zone were observed in both sample periods (Fig. 3a, b). In the lacustrine zone, undersaturation of CO_2 was prevalent at all sample sites in the rainy and dry seasons. Considering all of the sample sites, there were significant differences between the rainy and dry seasons ($t = 1.99$, $p < 0.05$). The Chl values were similar in the transition and lacustrine zone in the rainy season ($t = 2.01$, $p > 0.05$) and were higher in the transition zone during the dry season ($t = 2.01$, $p < 0.05$; Fig. 3a, b; Table 1). Furthermore, the average concentration in the transition zone was 2.5 times higher than the reservoir average (129.2 and 52.0 µg L^{-1}, respectively). Unlike the pCO_2, the Chl data showed no significant difference between the rainy and dry season considering all of the spatial data ($t = 1.99$, $p > 0.05$).

Table 1. Average CO_2 fluxes (mmol m^{-2} d^{-1}) calculated using spatial and temporal data. Positive fluxes denote net gas fluxes from the lake into the atmosphere. In the last column, the different letters represent significant differences (t test, $p < 0.05$). Lowercase letters represent differences between the fluxes in the reservoir zones, and uppercase letters represent the differences between the fluxes during the seasons.

		CO_2 fluxes mmol m^{-2} d^{-1}				
		k_{600} (MacIntyre et al., 2010)		k_{600} (Cole and Caraco, 1998)		
		Average	SD	Average	SD	Significant differences
	Area (km^2)	Spatial data				
Rainy summer						
Entire reservoir	36.0	−10.1	26.8	−7.2	21.9	
Riverine zone	5.7	44.5	6.5	37.6	5.5	a
Transition zone	9.3	−24.8	15.3	−19.1	11.7	b, e
Lacustrine zone	20.9	−18.3	9.1	−14.1	7.0	b
Dry winter						
Entire reservoir	34.3	24.6	61.5	22.1	50.8	
Riverine zone	13.7	93.0	13.3	78.7	11.2	c
Transition zone	7.6	−4.7	51.5	−2.0	42.1	d
Lacustrine zone	13.1	−29.7	18.1	−22.9	13.9	e
		At the dam				
All data throughout the year		−0.1	39.8	−0.9	33.1	
Rainy spring		−28.6	24.6	−27.1	18.5	A
Rainy summer		8.1	41.8	7.6	35.6	B
Dry autumn		23.7	39.2	19.6	29.9	C
Dry winter		−0.4	33.0	−0.6	25.5	D

The calculated CO_2 fluxes from the spatial data varied from −46.5 to 52.2 mmol m^{-2} d^{-1} and −61.9 to 103.16 mmol m^{-2} d^{-1} during the rainy and dry season, respectively. In both the rainy and dry seasons, the maximum emissions were observed in the riverine zone and the minimum was observed in the transition zone. The spatial average was −10.1 and 24.6 mmol m^{-2} d^{-1} during the rainy and dry season, respectively (Table 1).

3.2 Temporal variability

The pCO_2 calculated from the multi-parameter sonde data (temperature and pH) and the alkalinity showed a large seasonal variability over the year at the station near the dam (Table 2). The pCO_2 varied from 35 to 4058 µatm, with an average of 624 ± 829 µatm and median of 165 µatm. The pCO_2 supersaturation was prevalent between April and June, whereas pCO_2 undersaturation was prevalent during all other periods (Fig. 4a). The lowest median of pCO_2 was observed between October and December (43 µatm). Considering all of the temporal data throughout the year, 59.8 % of the data measured below atmospheric equilibrium and 1.1 % were within 5 % of the atmospheric equilibrium.

In the Funil Reservoir, the seasonal pCO_2 variation over the year at the station near the dam agreed with the variation in the retention time (Fig. 4). The yearly average of the reservoir retention time was 32.6 days over the research year. The lower retention time occurred between October and December, when the water level was low and the reservoir was ready to stock water coming from the watershed and rain during the rainy season (October to March).

Because we sampled temperature on a sub-daily scale over the year, we used the equations proposed by MacIntyre et al. (2010) to calculate k_{600}, which also incorporates the turbulence from heat loss. The turbulence from heat loss, especially overnight, often exceeds that from wind mixing in tropical lakes that tend to have low wind. However, the estimates using Cole and Caraco (1998) formulations to calculate k_{600} did not significantly change our results (Table 1). Due to the large sample size of the temporal data (hourly data), significant differences were observed between the estimates, primarily in the dry autumn, when the surface temperature decreased after the warm-summer ($t = 1.96$, $p < 0.05$). The CO_2 flux over the year at the station near the dam varied from −104.7 to 175.88 mmol m^{-2} d^{-1}. The average flux was -0.1 ± 39.8 mmol m^{-2} d^{-1} and the median was −7.4 mmol m^{-2} d^{-1}. We observed a substantial uptake of CO_2 between October and December (rainy spring) (Table 1). From January to July, the lake lost substantial CO_2 via degassing (Table 1). The uptake of CO_2 from the atmosphere

Table 2. Average and standard deviations of environmental and chemical variables from station S28 (near the dam) and river. *Cumulative precipitation over 3 months.

Months	Oct–Dec		Jan–Mar		Apr–Jun		Jul–Sep	
Season	Rainy autumn		Rainy summer		Dry spring		Dry winter	
	Average	SD	Average	SD	Average	SD	Average	SD
Air temperature (°C)	22.5	4.0	24.0	3.3	20.7	3.1	19.6	4.0
Alkalinity (mg L^{-1} as CaCO$_3$)	11.0	0.2	15.5	4.6	11.3	3.7	12.5	3.0
Chlorophyll (mg L^{-1})	12.9	12.8	23.8	20.6	3.0	0.2	23.2	35.0
Total phosphorus (µg L^{-1})	42.3	8.5	41.7	12.2	18.4	8.6	33.7	28.0
Total nitrogen (µg L^{-1})	1264.6	357.1	1143.2	305.3	1505.6	454.3	1203.3	299.7
Maximum depth (m)	65.1	1.8	69.3	1.4	71.6	2.5	69.1	4.4
Mean reservoir depth (m)	19.3	0.4	20.3	0.4	20.9	0.7	20.3	1.1
pCO$_2$ (µatm)	68.9	118.6	848.9	1027.5	1111.8	907.5	521.9	618.5
Precipitation (mm)*	547.0		420.2		230.2		71.6	
Retention time (days)	27.9	7.7	33.0	9.0	36.4	6.4	33.2	7.4
Max daily solar radiation (W m^{-2})	937.7	276.1	958.1	246.8	716.9	227.2	758.0	189.7
Surface water temperature (°C)	24.7	1.1	27.1	1.0	24.1	1.7	22.0	1.0
Wind speed (m s^{-1})	–	–	1.6	1.2	1.4	1.3	1.6	1.5
River total phosphorus (mg L^{-1})	80.6	–	77.1	–	42.4	–	88.3	–
River total nitrogen (mg L^{-1})	1535.5	–	2072.5	–	1524.2	–	1972.6	–
River total carbon (mg L^{-1})	12.9	2.0	13.3	1.8	13.7	2.5	12.1	2.9
Downstream total carbon (mg L^{-1})	12.4	2.3	11.8	0.3	13.7	2.6	11.9	1.6
Inflow (m^3 s^{-1})	224.2	58.9	236.4	74.1	234.1	36.7	168.9	28.7
Outflow (m^3 s^{-1})	223.6	57.2	236.4	74.1	226.0	30.9	219.1	10.7

* Cumulative precipitation over 3 months.
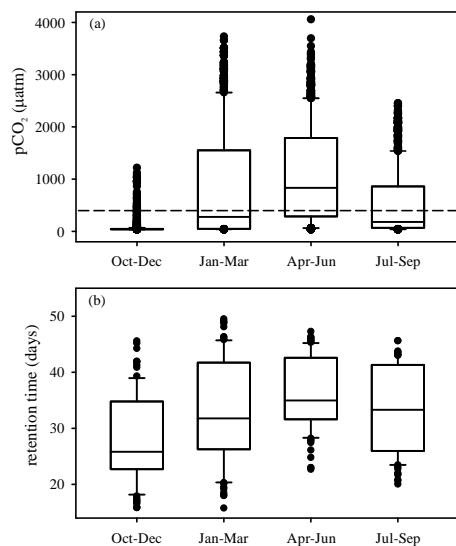
Figure 4. Box plot of the pCO$_2$ at station S28 near the dam **(a)** and the mean reservoir retention time **(b)** over the studied year. The dashed line represents the average pCO$_2$ in the atmosphere (375 µatm). The data are subdivided into four seasons: rainy spring (October–December), rainy summer (January–March), dry autumn (April–June) and dry winter (July–September).

was also prevalent between July and September (dry winter). A summary of all other data collected over the study period is shown in Table 2.

3.3 Thermal structure of the transition and riverine zone

We observed significant differences between the thermal structures during the rainy and dry season (Fig. 5). During the rainy season, thermal stratification only occurred in the transition zone during the daytime, at approximately 16:30 LT, when a maximum of 33.1 °C and a minimum of 27.8 °C was observed at the surface and bottom, respectively (Fig. 5a). In contrast, the temperature was vertically homogeneous at nighttime. The daily temperature oscillation during the rainy season at the surface reached up to 5 °C. During the dry season, the water temperature was lower compared to the rainy season in the transition zone. Stratification occurred at approximately 14:00 LT during the dry season, when we observed a maximum of 25.7 °C and a minimum of 23.1 °C at the bottom. The daily temperature oscillation reached up to 3 °C at the surface and stratus layers with different temperatures were observed every 2.5 m (Fig. 5b). The river temperature varied from 27.7 to 28.7 °C and 23.6 to 24.1 °C in the rainy and dry season, respectively (Table 3). The average temperature difference between the river and reservoir
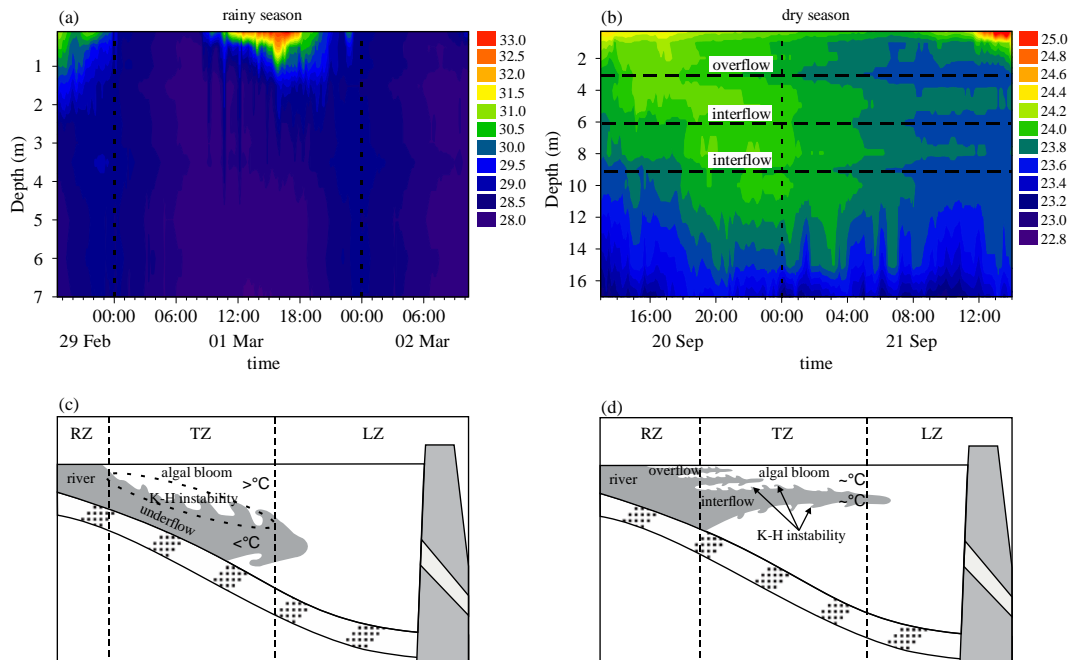
Figure 5. The temperature profile collected at station S09 during the rainy season **(a)** and at station S14 during the dry season **(b)**. The dashed line represents the depths where the river flows as overflow or interflows. During the rainy season, the river plunges and flows under the reservoir (underflow) due to differences in density **(c)**. The waves and billows develop along the interface due to the shear velocity (Kelvin–Helmholtz instability) and facilitate vertical mixing (see text). During the dry season, the river flows as overflow or interflow **(d)** because the difference in the density between the river and reservoir is low. In this situation, the river can influence the reservoir surface water more 5 km toward the dam. RZ: riverine zone; TZ: transition zone; LZ: lacustrine zone.

surface waters was 2.1 and 0.3 °C during the rainy and dry season, respectively.

3.4 Simulations

We first compared the simulated and real temperatures at stations S09 and S14 from the rainy and dry season, respectively. The RMSE, calculated by comparing the data every 20 min, was 1.4 °C for the rainy season and 1.1 °C for the dry season. These results, obtained for both seasons, were comparable with previous modeling exercises found in the literature (Jin et al., 2000; Vidal et al., 2012). We also analyzed the ability of the model to reproduce inflow, using data from drifters released in the riverine and transition zones of the reservoir from 1 March and 20 September (data not shown). Although the vertical thermal structures observed during the dry season (Fig. 5b) were not well represented, the model reproduced the behavior of the inflow as underflow during the rainy season (Fig. 6a) and as interflow and overflow during the dry season (Fig. 6b) as anticipated by the schematic representation (Fig. 5c, d). The river flowed mainly at 6 m depth near the bottom of the Funil Reservoir after the river plunge point during the rainy season. During the dry season, the river flowed mainly at 3 m depth at night and 4 m during the daytime.

The daily oscillation of the neutral buoyancy observed occurs because of the variation of the reservoir surface and river temperatures (Vidal et al., 2012, Curtarelli et al., 2013). The level of neutral buoyancy, where the densities of the flowing current and the ambient fluid are equal, represents the depth at which the river water spreads laterally in the reservoir. During the rainy season, the river flowed as underflow (Fig. 6a); however, when the river reached its maximum temperature, at approximately 21:00 LT (Table 3), the temperature difference between the river and surface water decreased, the level of river neutral buoyancy moved upward and the maximum flow was observed between 4 and 6 m (Fig. 6a). During the dry season, the river overflowed, but it plunged down to 4 to 6 m depth when high surface temperatures during the day coincided with a period of the lowest river temperatures (Table 3) and neutral buoyancy moved downward (Fig. 6b). The change in river flow patterns between September 20 and 21 occurred due to a decrease in the river temperature during a rainfall that occurred at approximately 16:00 LT on 20 September 2012 (Fig. 6b).

Table 3. Average of the hourly temperature profile collected by the thermistor chain located at station S05 (river) on 29 February 2012 (rainy season) and 20 September 2012 (dry season).

Rainy season					
Hour (LT)	River temp. (°C)		Hour (LT)	River temp. (°C)	
	Average	SD		Average	SD
00:00	28.39	0.04	12:00	27.71	0.03
01:00	28.28	0.04	13:00	27.72	0.04
02:00	28.17	0.05	14:00	27.79	0.11
03:00	28.07	0.03	15:00	27.97	0.06
04:00	28.00	0.02	16:00	28.03	0.02
05:00	27.91	0.04	17:00	28.16	0.09
06:00	27.85	0.04	18:00	28.34	0.09
07:00	27.77	0.05	19:00	28.49	0.06
08:00	27.73	0.00	20:00	28.63	0.04
09:00	27.72	0.01	21:00	28.70	0.01
10:00	27.71	0.02	22:00	28.67	0.03
11:00	27.69	0.01	23:00	28.55	0.05
Max			28.70 (21:00)		
Min			27.69 (11:00)		
Dry season					
Hour (LT)	River temp. (°C)		Hour (LT)	River temp. (°C)	
	Average	SD		Average	SD
00:00	23.90	0.02	12:00	23.80	0.08
01:00	23.88	0.02	13:00	23.82	0.02
02:00	23.80	0.06	14:00	23.87	0.04
03:00	23.74	0.04	15:00	23.89	0.04
04:00	23.71	0.04	16:00	24.00	0.04
05:00	23.66	0.01	17:00	23.97	0.05
06:00	23.64	0.01	18:00	23.99	0.08
07:00	23.60	0.04	19:00	24.08	0.02
08:00	23.57	0.03	20:00	24.03	0.02
09:00	23.59	0.01	21:00	24.00	0.02
10:00	23.62	0.02	22:00	23.96	0.02
11:00	23.65	0.02	23:00	23.95	0.02
Max			24.08 (19:00)		
Min			23.57 (08:00)		

4 Discussion

4.1 pCO$_2$ driven by phytoplankton

Primary production associated with high Chl levels was the main regulator of the CO$_2$ concentration at the surface of the Funil Reservoir (Fig. 7). Spatially, the pCO$_2$ levels were negatively correlated with the Chl ($r^2 = 0.71$). In old hydropower reservoirs, where the C source from flooded soil after impounding has become negligible, primary production may become a significant element of the C budget. Intense primary production fueled by high levels of nutrients reduces the CO$_2$ concentrations to levels below the atmospheric equilibrium in transition and lacustrine zones of the Funil Reservoir (Fig. 3). The high pCO$_2$ in the riverine zone may be explained by the terrestrial ecosystem respiration entering the river as dissolved soil CO$_2$, the oxidation of allochthonous and emergent autochthonous organic carbon, the acidification of buffered waters, the precipitation of carbonate min-

erals, and the direct pumping of root respiration CO$_2$ from riparian vegetation (Butman and Raymond, 2011).

Low pCO$_2$ levels observed at the station near the dam over the year was associated with the following: (1) high primary production due to higher temperatures and solar radiation that promoted water column stability and stratification and (2) constant high nutrient availability. Because nutrient availability in the Funil Reservoir was high during the entire year (Table 2), the phytoplankton growth was not limited by nutrients in the lacustrine zone. However, seasonal variation in factors that control stability and stratification, such as temperature, wind and mixing zone depth, may inhibit algal growth near the dam, especially between April and June.

Due to phytoplankton productivity, we observed a net uptake of CO$_2$ over the year at the station near the dam, especially between October and December (Table 1). However, the fate of carbon fixed by phytoplankton in the Funil Reservoir is still unclear. The higher flux of methane (CH$_4$) from sediment to water that was observed in the Funil Reservoir compared with other tropical reservoir (Ometto et al., 2013) suggests that a substantial fraction of the carbon fixed by the phytoplankton reached the sediment and was further mineralized as CH$_4$. However, in the lacustrine zone, the higher depth and high temperatures may promote the decomposition of dead phytoplankton generating CO$_2$ or CH$_4$ in the water column before it reaches the sediment.

It is important to note that the CO$_2$ production in the sediments can leave an imprint on the pCO$_2$ of the surface water, especially in the dry season, when the reservoir is not stratified. During periods of water stratification, the carbon coming from organic carbon mineralization in the sediment may be trapped in the hypolimnion and may not contribute to the CO$_2$ flux from the water to the atmosphere (Cardoso et al., 2013). Furthermore, it is important to highlight that the contribution of carbon mineralization in the sediment to the pCO$_2$ at the surface can also be regulated by other factors such as CO$_2$ saturation in the water and the depth of the reservoir (Guérin et al., 2006). Moreover, when the river plunges and flows at the bottom of the reservoir, the water flow can disturb the sediment and enhance the carbon flux from the sediment to the hypolimnion, which can affect the contribution of organic carbon mineralized on the sediment to the amount of carbon emitted by the reservoir.

By considering that the outflow exported the same amount of carbon as that from the watershed (Table 2), we suggest that a high sedimentation rate offsets the uptake of CO$_2$ from the atmosphere to close the carbon budget. Although there are no data to support this statement, we hypothesize that both (i) the burial of organic carbon composed of phytoplankton and (ii) methanogenesis are important carbon pathways for the carbon fixed by the phytoplankton in the Funil Reservoir, as reported in natural eutrophic lakes (Downing et al., 2008).
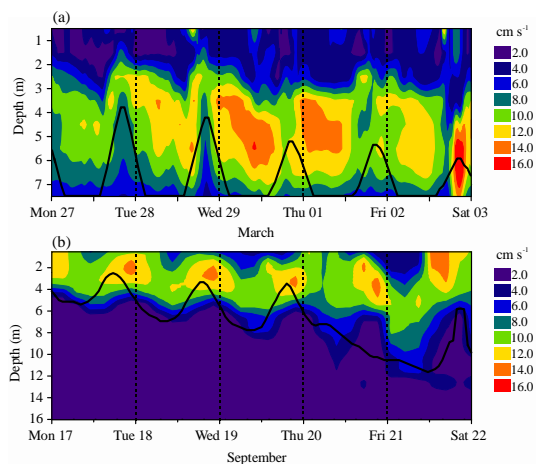
Figure 6. Simulated velocity profile using realistic forcing. Higher velocities represent the depth where the river flows though the transition zone. The river flows as underflow during the rainy season when a denser (colder) river plunges beneath the surface and flows downward along the bottom as a gravity-driven density current **(a)**. The river flows as overflow during the dry season, when the temperature from the river and reservoir are similar **(b)**. As overflow, the river characteristics can be found many kilometers toward the dam at the water surface. The black line represents the depth of neutral buoyancy as estimated from temperature records, presuming that the lake and river water do not mix. The anomaly observed in the river flow and depth of neutral buoyancy between 20 and 21 September 2012 occurred due to a decrease in the river temperature during a rainfall that occurred at approximately 16:00 LT on 20 September.

Figure 7. Relationship between the spatial pCO_2 and Chl data in the Funil Reservoir. The regression is represented by a dashed line ($r^2 = 0.71$, $p < 0.001$).

4.2 Physical features and spatial distribution

The Funil Reservoir's retention time is strongly driven by the operation of the dam. The volume of water that flows through the turbine depends on the energy demands and inflow from the Paraíba do Sul River. Periods of low retention time and water levels do not necessarily correspond to periods of low precipitation. In fact, the highest retention time and water level is often observed in the middle of the dry season, when the reservoir is full to ensure enough water to produce energy during the entire dry season. This suggests that these processes are not only driven by natural factors but that they may also be regulated by dam operation in the Funil Reservoir.

The position of the transition zone of the reservoir moves as a result of the season (Fig. 3). At the end of the rainy season, the retention time and water level was high and the influence of the river in the surface water of the reservoir was restricted to a small area (Fig. 2a, c). However, when the water level and retention time was low, the transition zone moved toward the dam and the river inflow influenced the surface Chl and pCO_2 over more than 40 % of the total reservoir surface area (Fig. 2b, d). As previously reported, when the reten-
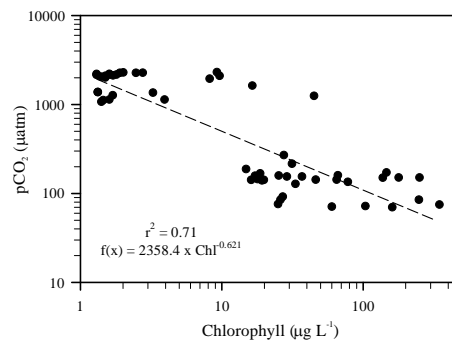
tion time is short, a reservoir can become a fluvial-dominated system (Straškraba, 1990).

The size of the river-influenced area over the reservoir surface water also depends on the water density. Differences in the river and reservoir temperatures, the total dissolved solids, and the suspended solids can cause a density gradient in the water column. Depending on the water density differences between the inflow and the reservoir, the river can flow into the downstream area as overflow, underflow or interflow (Martin and McCutcheon, 1998). During the rainy season in the Funil Reservoir, due to the substantial difference between the river and reservoir surface temperatures ($\sim 4\,°C$), the river water progressively sinks down (underflow) and contributes to the thermal stability of the water column (Fig. 5a, Assireu et al., 2011). The denser river water flows under the lighter reservoir water and waves and billows develop along the interface due to the shear velocity. This behavior is indicative of Kelvin–Helmholtz instability, in which waves made up of fluid from the current (river) promote mixing with the reservoir water (Thorpe and Jiang, 1998; Corcos and Sherman, 2005) (Fig. 5c). This mixing, and the high nutrient concentration coming from Paraíba do Sul River (Table 2), may explain the high Chl levels observed in the transition zone (Fig. 3).

Many cold fronts pass through the Brazilian midwest and southeast during the dry seasons. (Lorenzzetti et al., 2005, Alcântara et al., 2010). As a result, the decrease in the reservoir surface temperature (Table 2) and consequent decrease in the density difference between the river and reservoir surfaces leads to river inflow that is characterized by inter-overflow (Fig. 5b, d). In an inter-overflow, the riverine characteristics of high turbulence, pCO_2 and low Chl are observed in the reservoir surface 5 km toward the dam (Fig. 3a, b). Although there are high nutrient concentrations in the transition zone (Table 1) between S19 and the river, the surface water is dominated by river flow with low Chl concentrations (Fig. 3). Favorable conditions for phytoplankton blooming will only exist down-reservoir in the transition

Table 4. Comparison between CO_2 fluxes ($\text{mmol m}^{-2}\,\text{d}^{-1}$) calculated during periods of low retention time and high retention time. Positive fluxes denote net gas fluxes from the lake to the atmosphere. Statistical analyses showed significant differences between temporal and spatial data and between low and high retention times (*t* test, $p < 0.05$). * We considered data for low retention and high retention time as values less than 25 days and more than 38 days, respectively. The average CO_2 fluxes during periods of intermediate retention time were close to 0 ($0.5\,\text{mmol m}^{-2}\,\text{d}^{-1}$).

	CO_2 fluxes $\text{mmol m}^{-2}\,\text{d}^{-1}$			
	Low retention time		High retention time	
	Average	SD	Average	SD
Temporal data	−18.6	30.3	14.5	33.6
Spatial data	24.6	61.5	−10.1	26.8

zone, where the inflow mixes with the reservoir and loses velocity (Vidal et al., 2012).

The simulation of the rainy season (Fig. 6) indicated a minimal influence from the river inflow on the surface water, which was suggested by the thermal stability in the transition zone (Fig. 5a). The simulation of the dry season represented the overflow, particularly at night (Fig. 6b). However, the simulation did not represent intrusions of the river water on the different depths (every 2.5 m) as suggested by the temperature profile in the transition zone (Fig. 5b). The variation in the river inflow over the day (Fig. 6) occurred in response to the lag change in the temperature of the river and the reservoir. During the rainy season, this oscillation enhanced the intake of nutrients into the euphotic zone when the reservoir surface temperature decreased and the river temperature reached its maximum at the end of the day (Table 3). During the day, when the river temperature dropped, the large peak of Chl in the transition zone (Fig. 3a) could be a result of developing diurnal stratification (Fig. 5). During the dry season, peak Chl occurs 5 km further downstream (Fig. 3b) because the inflow never plunges due to lower temperature differences between the river and reservoir surfaces.

4.3 Spatial and temporal heterogeneity

As a result of the phytoplankton growth associated with these physical features, there are large spatial and temporal variations in the CO_2 fluxes in the Funil Reservoir. Several studies of hydropower reservoirs have suggested that significant CO_2 is emitted from these systems into the atmosphere at a global scale (St Louis et al., 2000; Roehm and Tremblay, 2006; Barros et al., 2011; Fearnside and Pueyo, 2012). However, recent studies have shown that the growing nutrient enrichment caused by human activities (eutrophication) can reverse this pattern in some hydropower reservoirs (Roland et al., 2010) and natural lakes (Pacheco et al., 2014). Our study indicates that the Funil Reservoir is spatially heterogeneous,

with high CO_2 emissions in the riverine zone and high CO_2 uptake in the transition and lacustrine zones. Temporally, the reservoir near the dam is undersaturated in pCO_2 mainly between October and December (wet season) and is supersaturated in pCO_2 between April and June (dry season, Table 1). Similarly, higher values of pCO_2 were previously reported during the dry season in the Funil Reservoir (Roland et al., 2010).

We could have different or opposite conclusions if the spatial and temporal pCO_2 data were analyzed separately. Previous studies have suggested that, in natural small lakes, a single sample site would be adequate to determine whether a lake is above or below equilibrium with the atmosphere and the intensity of the fluxes (Kelly et al., 2001). However, large spatial heterogeneity of pCO_2 and CO_2 emissions into the atmosphere have been observed in boreal (Teodoru et al., 2011) and tropical (Roland et al., 2010) reservoirs. Our temporal data at the dam station exhibited lower pCO_2 in October, November and December, when the retention time was extremely low (Table 4); however, this observation did not represent the entire reservoir. The spatial data collected at low water levels showed low pCO_2 in the dam as well; however, almost half of the reservoir is supersaturated due to river influences (Fig. 2d). The average pCO_2 during low retention time was $881\,\mu\text{atm}$ over the whole reservoir area, contrasting with only $69\,\mu\text{atm}$ near the dam. Furthermore, if we considered only one station near the dam to estimate the CO_2 flux between the lake surface and atmosphere, the conclusion would be contradictory. For example, during periods of low retention time, the calculated CO_2 flux indicated that the CO_2 flux would be $-17.6\,\text{mmol m}^{-2}\,\text{d}^{-1}$ (CO_2 sink) for one-spot temporal data and $22.1\,\text{mmol m}^{-2}\,\text{d}^{-1}$ (CO_2 source) for the whole reservoir (Table 4).

The same contradictory conclusions can be expressed when studies with low sample site numbers are considered for spatial heterogeneity. Previous studies looking at the heterogeneity of the Funil Reservoir indicated no phytoplankton biomass peak in the transition zone (Soares et al., 2012). In our study, the Chl data collected every 1000 m as a proxy were able to show a clear transition zone within the reservoir. Furthermore, data analysis in Soares et al. (2012), considering four sampling stations, exhibited high spatial heterogeneity in periods of high retention times (high water level). In contrast, we found high spatial heterogeneity in low retention times, corresponding to periods of high influence from the river on the surface water. Thus, the different conclusions in Soares et al. (2012) may be explained by the variation in the spatial distribution of the transition zone location once the retention time and inflow are used as key parameters to define its location (Fig. 2c, d).

5 Conclusions

In summary, the seasonal and spatial variability of the Chl and CO_2 fluxes in the Funil Reservoir are mainly related to river inflow and retention times. However, the relationship between the pCO_2 and Chl suggests that primary production regulates the surface CO_2 fluxes in the transition and lacustrine zone. The average spatial data showed CO_2 emissions into the atmosphere during periods of low retention time (even with higher Chl) due to the river's influence on the surface water and CO_2 uptake during periods of high retention time when the river plunges and flows under the reservoir. However, the retention time threshold that seals the transition between a source and sink of CO_2 could not be determined. A comparison between the spatial (42 stations) and temporal data (1 station) indicated that different conclusions may be drawn if spatial heterogeneity is not adequately considered. Furthermore, transition zone location changes over the year must be considered when a low number of stations are used to represent spatial heterogeneity. The lack of spatial information about CO_2 fluxes could lead to erroneous conclusions about the importance of hydropower reservoirs in the freshwater carbon cycle. The Funil Reservoir is a dynamic system where the hydrodynamics linked to the river inflow and retention time control both pCO_2 and Chl spatial variability and seem to regulate most ecological processes.

References

Abril, G., Guerin, F., Richard, S., Delmas, R., Galy-Lacaux, C., Gosse, P., Tremblay, A., Varfalvy, L., Dos Santos, M. A., and Matvienko, B.: Carbon dioxide and methane emissions and the carbon budget of a 10-year old tropical reservoir (Petit Saut, French Guiana), Global Biogeochem. Cy., 19, GB4007, doi:10.1029/2005gb002457, 2005.

Abril, G., Richard, S., and Guerin, F.: In situ measurements of dissolved gases (CO_2 and CH_4) in a wide range of concentrations in a tropical reservoir using an equilibrator, Sci. Total Environ., 354, 246–251, doi:10.1016/j.scitotenv.2004.12.051, 2006.

Abril, G., Parize, M., Perez, M. A. P., and Filizola, N.: Wood decomposition in Amazonian hydropower reservoirs: An additional source of greenhouse gases, J. S. Am. Earth Sci., 44, 104–107, doi:10.1016/j.jsames.2012.11.007, 2013.

Abril, G., Martinez, J.-M., Artigas, L. F., Moreira-Turcq, P., Benedetti, M. F., Vidal, L., Meziane, T., Kim, J.-H., Bernardes, M. C., Savoye, N., Deborde, J., Souza, E. L., Alberic, P., Landim de Souza, M. F., and Roland, F.: Amazon River carbon dioxide outgassing fuelled by wetlands, Nature, 505, 395–398, doi:10.1038/nature12797, 2014.

Ackerman, S. A., Strabala, K. I., Menzel, W. P., Frey, R. A., Moeller, C. C., and Gumley, L. E.: Discriminating clear sky from clouds with MODIS, J. Geophys. Res.-Atmos., 103, 32141–32157, doi:10.1029/1998JD200032, 1998.

AGEVAP: Relatório Técnico - Bacia do Rio Paraíba Do Sul - Subsídios às Ações de Melhoria da Gestão 2011, Associação Pró-Gestão das Águas da Bacia Hidrográfica do Rio Paraíba do Sul, 255, Resende, 2011.

Akaike, H.: New look at statistical-model identification, IEEE T. Automat. Contr., 19, 716–723, doi:10.1109/tac.1974.1100705, 1974.

Alcantara, E., Curtarelli, M., Ogashawara, I., Stech, J., and Souza, A.: Hydrographic observations at SIMA station Itumbiara in 2013, in: Long-term environmental time series of continuously collected data in hydroelectric reservoirs in Brazil, edited by: Alcantara, E., Curtarelli, M., Ogashawara, I., Stech, J., and Souza, A., PANGAEA, Bremerhaven, 1–3, 2013.

Alcântara, E. H., Bonnet, M. P., Assireu, A. T., Stech, J. L., Novo, E. M. L. M., and Lorenzzetti, J. A.: On the water thermal response to the passage of cold fronts: initial results for Itumbiara reservoir (Brazil), Hydrol. Earth Syst. Sci. Discuss., 7, 9437–9465, doi:10.5194/hessd-7-9437-2010, 2010.

APHA: Standard Methods for the Examination of Water and Wastewater, 21 ed., Washington, DC, 1368 pp., 2005.

Assireu, A. T., Alcântara, E., Novo, E. M. L. M., Roland, F., Pacheco, F. S., Stech, J. L., and Lorenzzetti, J. A.: Hydrophysical processes at the plunge point: an analysis using satellite and in situ data, Hydrol. Earth Syst. Sci., 15, 3689–3700, doi:10.5194/hess-15-3689-2011, 2011.

Bailey, T. C. and Gatrell, A. C.: Interactive spatial data analysis, in, Essex: Longman Scientific & Technical, 432 pp., 1995.

Barros, N., Cole, J. J., Tranvik, L. J., Prairie, Y. T., Bastviken, D., Huszar, V. L. M., del Giorgio, P., and Roland, F.: Carbon emission from hydroelectric reservoirs linked to reservoir age and latitude, Nat. Geosci., 4, 593–596, doi:10.1038/Ngeo1211, 2011.

Borges, A. V., Vanderborght, J.-P., Schiettecatte, L. S., Gazeau, F., Ferrón-Smith, S., Delille, B., and Frankignoulle, M.: Variability of the gas transfer velocity of CO_2 in a macrotidal estuary (the Scheldt), Estuaries, 27, 593–603, doi:10.1007/BF02907647, 2004.

Branco, C. W. C., Rocha, M. I. A., Pinto, G. F. S., Gômara, G. A., and Filippo, R.: Limnological features of Funil Reservoir (R.J., Brazil) and indicator properties of rotifers and cladocerans of the zooplankton community, Lakes Reserv. Res. Manag., 7, 87–92, doi:10.1046/j.1440-169X.2002.00177.x, 2002.

Butman, D. and Raymond, P. A.: Significant efflux of carbon dioxide from streams and rivers in the United States, Nat. Geosci., 4, 839–842, doi:10.1038/ngeo1294, 2011.

Câmara, G., Souza, R. C. M., Freitas, U. M., and Garrido, J.: Spring: Integrating remote sensing and gis by object-oriented data modelling, Comput. Graph., 20, 395–403, doi:10.1016/0097-8493(96)00008-8, 1996.

Cardoso, S. J., Vidal, L. O., Mendonça, R. F., Tranvik, L. J., Sobek, S., and Roland, F.: Spatial variation of sediment mineralization supports differential CO_2 emissions from a tropical hydroelectric reservoir, Front. Microbiol., 4, 101, doi:10.3389/fmicb.2013.00101, 2013.

Casulli, V. and Cheng, R. T.: Semiimplicit Finite-Difference Methods for 3-Dimensional Shallow-Water Flow, Int. J. Numer. Meth. Fl., 15, 629–648, doi:10.1002/fld.1650150602, 1992.

Cole, J. J. and Caraco, N. F.: Atmospheric exchange of carbon dioxide in a low-wind oligotrophic lake measured by the addition of SF6, Limnol. Oceanogr., 43, 647–656, 1998.

Corcos, G. M. and Sherman, F. S.: The mixing layer: deterministic models of a turbulent flow, J. Fluid Mech., 139, 29–65, 2005.

Curtarelli, M. P., Alcântara, E., Renno, C. D., Assireu, A. T., Stech, J. L., and Bonnet, M. P.: Modelling the surface circulation and thermal structure of a tropical reservoir using three-dimensional hydrodynamic lake model and remote-sensing data, Water Environ. J., 28, 516–525, 2013.

Demarty, M., Bastien, J., and Tremblay, A.: Annual follow-up of gross diffusive carbon dioxide and methane emissions from a boreal reservoir and two nearby lakes in Québec, Canada, Biogeosciences, 8, 41–53, doi:10.5194/bg-8-41-2011, 2011.

Di Siervi, M. A., Mariazzi, A. A., and Donadelli, J. L.: Bacterioplankton and phytoplankton production in a large Patagonian reservoir (Republica Argentina), Hydrobiologia, 297, 123–129, 1995.

Downing, J. A., Cole, J. J., Middelburg, J. J., Striegl, R. G., Duarte, C. M., Kortelainen, P., Prairie, Y. T., and Laube, K. A.: Sediment organic carbon burial in agriculturally eutrophic impoundments over the last century, Global Biogeochem. Cy., 22, Gb1018, doi:10.1029/2006gb002854, 2008.

Fearnside, P. M. and Pueyo, S.: Greenhouse-gas emissions from tropical dams, Nature Clim. Change, 2, 382–384, 2012.

Finlay, K., Leavitt, P. R., Wissel, B., and Prairie, Y. T.: Regulation of spatial and temporal variability of carbon flux in six hard-water lakes of the northern Great Plains, Limnol. Oceanogr., 54, 2553–2564, doi:10.4319/lo.2009.54.6_part_2.2553, 2009.

Finlay, K., Leavitt, P. R., Patoine, A., and Wissel, B.: Magnitudes and controls of organic and inorganic carbon flux through a chain of hard-water lakes on the northern Great Plains, Limnol. Oceanogr., 55, 1551–1564, doi:10.4319/lo.2010.55.4.1551, 2010.

Fischer, H. B. and Smith, R. D.: Observations of transport to surface waters from a plunging inflow to Lake Mead, Limnol. Oceanogr., 28, 258–272, 1983.

Fischer, H. B., List, E. J., Koh, R. C. Y., Imberger, J., and Brooks, N. H.: Mixing in inland and coastal waters, Academic Press, New York, 483 pp., 1979.

Ford, D. E.: Reservoir Transport Processes, in: Reservoir Limnology: Ecological Perspectives, edited by: Thornton, K. W., Kimmel, B. L., and Payne, F. E., Wiley-Interscience, New York, 15–41, 1990.

Gippel, C. J.: The use of turbidimeters in suspended sediment research, Hydrobiologia, 176, 465–480, doi:10.1007/bf00026582, 1989.

Guérin, F., Abril, G., Richard, S., Burban, B., Reynouard, C., S eyler, P., and Delmas, R.: Methane and carbon dioxide emissions from tropical reservoirs: Significance of downstream rivers, Geophys. Res. Lett., 33, L21407, doi:10.1029/2006GL027929, 2006.

Halbedel, S. and Koschorreck, M.: Regulation of CO_2 emissions from temperate streams and reservoirs, Biogeosciences, 10, 7539–7551, doi:10.5194/bg-10-7539-2013, 2013.

Hodges, B. R., Imberger, J., Saggio, A., and Winters, K. B.: Modeling basin-scale internal waves in a stratified lake, Limnol. Oceanogr., 45, 1603–1620, 2000.

IBGE: Instituto Brasileiro de Geografia e Estatística. Censo Demográfico 2010, Rio de Janeiro, 2010.

Imberger, J. and Patterson, J. C.: Physical Limnology, Adv. Appl. Mech., 27, 303–475, 1990.

Jahne, B., Munnich, K. O., Bosinger, R., Dutzi, A., Huber, W., and Libner, P.: On the parameters influencing air-water gas-exchange, J. Geophys. Res.-Oceans, 92, 1937–1949, doi:10.1029/JC092iC02p01937, 1987.

Jin, K., Hamrick, J., and Tisdale, T.: Application of Three-Dimensional Hydrodynamic Model for Lake Okeechobee, J. Hydraul Eng., 126, 758–771, doi:10.1061/(ASCE)0733-9429(2000)126:10(758), 2000.

Justice, C. O., Vermote, E., Townshend, J. R. G., DeFries, R., Roy, D. P., Hall, D. K., Salomonson, V. V., Privette, J. L., Riggs, G., Strahler, A., Lucht, W., Myneni, R. B., Knyazikhin, Y., Running, S. W., Nemani, R. R., Zhengming, W., Huete, A. R., Van Leeuwen, W., Wolfe, R. E., Giglio, L., Muller, J. P., Lewis, P., and Barnsley, M. J.: The Moderate Resolution Imaging Spectroradiometer (MODIS): land remote sensing for global change research, IEEE T. Geosci. Remote Sens., 36, 1228–1249, doi:10.1109/36.701075, 1998.

Kelly, C. A., Fee, E., Ramlal, P. S., Rudd, J. W. M., Hesslein, R. H., Anema, C., and Schindler, E. U.: Natural variability of carbon dioxide and net epilimnetic production in the surface waters of boreal lakes of different sizes, Limnol. Oceanogr., 46, 1054–1064, 2001.

Kemenes, A., Forsberg, B. R., and Melack, J. M.: CO_2 emissions from a tropical hydroelectric reservoir (Balbina, Brazil), J. Geophys. Res.-Biogeo., 116, G03004, doi:10.1029/2010jg001465, 2011.

Kennedy, R. H.: Reservoir design and operation: limnological implications and management opportunities, in: Theoretical reservoir ecology and its applications, edited by: Tundisi, J. G. and Straškraba, M., Backhuys Publishers, Leiden, 1–28, 1999.

Klapper, H.: Water quality problems in reservoirs of Rio de Janeiro, Minas Gerais and Sao Paulo, Int. Rev. Hydrobiol., 83, 93–101, 1998.

Lauster, G. H., Hanson, P. C., and Kratz, T. K.: Gross primary production and respiration differences among littoral and pelagic habitats in northern Wisconsin lakes, Can. J. Fish. Aquat. Sci., 63, 1130–1141, doi:10.1139/f06-018, 2006.

Leonard, B. P.: The Ultimate Conservative Difference Scheme Applied to Unsteady One-Dimensional Advection, Comput. Method. Appl. M., 88, 17–74, doi:10.1016/0045-7825(91)90232-U, 1991.

Lorenzzetti, J. A., Stech, J. L., Assireu, A. T., Novo, E. M. L. D., and Lima, I. B. T.: SIMA: a near real time buoy acquisition and telemetry system as a support for limnological studies., in: Global warming and hydroelectric reservoirs., edited by: Santos, M. A. and Rosa, L. P., COPPE, Rio de Janeiro, 71–79, 2005.

MacIntyre, S., Jonsson, A., Jansson, M., Aberg, J., Turney, D. E., and Miller, S. D.: Buoyancy flux, turbulence, and the gas transfer

coefficient in a stratified lake, Geophys Res Lett, 37, L24604, doi:10.1029/2010GL044164, 2010.

Martin, J. L. and McCutcheon, S. C.: Hydrodynamics and Transport for Water Quality Modeling, CRC Press, Boca Raton, 1998.

Millero, F. J., Pierrot, D., Lee, K., Wanninkhof, R., Feely, R., Sabine, C. L., Key, R. M., and Takahashi, T.: Dissociation constants for carbonic acid determined from field measurements, Deep-Sea Res. Pt.-I, 49, 1705–1723, doi:10.1016/s0967-0637(02)00093-6, 2002.

Ometto, J. P., Cimbleris, A. C. P., dos Santos, M. A., Rosa, L. P., Abe, D., Tundisi, J. G., Stech, J. L., Barros, N., and Roland, F.: Carbon emission as a function of energy generation in hydroelectric reservoirs in Brazilian dry tropical biome, Energ. Policy, 58, 109–116, doi:10.1016/j.enpol.2013.02.041, 2013.

Ometto, J. P. H. B., Pacheco, F. S., Cimbleris, A. C. P., Stech, J. L., Lorenzzetti, J., Assireu, A. T., Santos, M. A., Matvienko, B., Rosa, L. P., Sadigisgalli, C., Donato, A., Tundisi, J. G., Barros, N. O., Mendonca, R., and Roland, F.: Carbon Dynamic and Emissions in Brazilian Hydropower Reservoirs, in: Energy Resources: Development, Distribution and Exploitation, edited by: Alcantara, E., Nova Science Publishers, Hauppauge, 155–188, 2011.

Pacheco, F. S., Assireu, A. T., and Roland, F.: Drifters tracked by satellite applied to freshwater ecosystems: study case in Manso Reservoir, in: New technologies for the monitoring and study of large hydroelectric reservoirs and lakes, edited by: Alcantara, E. H., Stech, J. L., and Novo, E. M. L. M., Parêntese, Rio de Janeiro, 193–218, 2011.

Pacheco, F. S., Roland, F., and Downing, J. A.: Eutrophication reverses whole-lake carbon budgets, Inland Waters, 4, 41–48, doi:10.5268/iw-4.1.614, 2014.

Rangel, L. M., Silva, L. H. S., Rosa, P., Roland, F., and Huszar, V. L. M.: Phytoplankton biomass is mainly controlled by hydrology and phosphorus concentrations in tropical hydroelectric reservoirs, Hydrobiologia, 693, 13–28, doi:10.1007/s10750-012-1083-3, 2012.

Richardot, M., Debroas, D., Jugnia, L. B., Tadonleke, R., Berthon, L., and Devaux, J.: Changes in bacterial processing and composition of dissolved organic matter in a newly-flooded reservoir (a three-year study), Arch. Hydrobiol., 148, 231–248, 2000.

Rocha, M. I. A., Branco, C. W. C., Sampaio, G. F., Gômara, G. A., and de Filippo, R.: Spatial and temporal variation of limnological features, Microcystis aeruginosa and zooplankton in a eutrophic reservoir (Funil Reservoir, Rio de Janeiro), Acta Limnol. Bras., 14, 73–86, 2002.

Roehm, C., and Tremblay, A.: Role of turbines in the carbon dioxide emissions from two boreal reservoirs, Quebec, Canada, J. Geophys. Res.-Atmos., 111, D24101, doi:10.1029/2006jd007292, 2006.

Roland, F., Vidal, L. O., Pacheco, F. S., Barros, N. O., Assireu, A., Ometto, J. P. H. B., Cimbleris, A. C. P., and Cole, J. J.: Variability of carbon dioxide flux from tropical (Cerrado) hydroelectric reservoirs, Aquat. Sci., 72, 283–293, doi:10.1007/s00027-010-0140-0, 2010.

Rosa, L. P., dos Santos, M. A., Matvienko, B., dos Santos, E. O., and Sikar, E.: Greenhouse gas emissions from hydroelectric reservoirs in tropical regions, Climatic Change, 66, 9–21, doi:10.1023/B:Clim.0000043158.52222.Ee, 2004.

Serra, T., Vidal, J., Casamitjana, X., Soler, M., and Colomer, J.: The role of surface vertical mixing in phytoplankton distribution in a stratified reservoir, Limnol. Oceanogr., 52, 620–634, 2007.

Slater, P. G.: Remote sensing, optics and optical systems, Addison-Wesley Pub. Co., Reading, 575 pp., 1980.

Smith, S. V.: Physical, chemical and biological characteristics of CO_2 gas flux across the air water interface, Plant Cell Environ., 8, 387–398, doi:10.1111/j.1365-3040.1985.tb01674.x, 1985.

Soares, M. C. S., Marinho, M. M., Huszar, V. L. M., Branco, C. W. C., and Azevedo, S. M. F. O.: The effects of water retention time and watershed features on the limnology of two tropical reservoirs in Brazil, Lakes Reserv. Res. Manag., 13, 257–269, doi:10.1111/j.1440-1770.2008.00379.x, 2008.

Soares, M. C. S., Marinho, M. M., Azevedo, S. M. O. F., Branco, C. W. C., and Huszar, V. L. M.: Eutrophication and retention time affecting spatial heterogeneity in a tropical reservoir, Limnologica – Ecology and Management of Inland Waters, 42, 197–203, doi:10.1016/j.limno.2011.11.002, 2012.

Spigel, R. H. and Imberger, J.: The Classification of Mixed-Layer Dynamics in Lakes of Small to Medium Size, J. Phys. Oceanogr., 10, 1104–1121, doi:10.1175/1520-0485(1980)010<1104:Tcomld>2.0.Co;2, 1980.

Staehr, P. A., Christensen, J. P. A., Batt, R. D., and Read, J. S.: Ecosystem metabolism in a stratified lake, Limnol. Oceanogr., 57, 1317–1330, doi:10.4319/lo.2012.57.5.1317, 2012.

Stevenson, M. R., Lorenzzetti, J. A., Stech, J. L., and Arlino, P. R. A.: SIMA – An Integrated Environmental Monitoring System, VII Simpósio Brasileiro de Sensoriamento Remoto, Curitiba, 10–14 May, 1993.

St Louis, V. L., Kelly, C. A., Duchemin, E., Rudd, J. W. M., and Rosenberg, D. M.: Reservoir surfaces as sources of greenhouse gases to the atmosphere: A global estimate, Bioscience, 50, 766–775, 2000.

Straškraba, M.: Retention time as a key variable of reservoir limnology, in: Theoretical reservoir ecology and its applications, edited by: Tundisi, T. G., and Straškraba, M., Backhuys Publishers, Leiden, 43–70, 1990.

Teodoru, C. R., Prairie, Y. T., and del Giorgio, P. A.: Spatial Heterogeneity of Surface CO_2 Fluxes in a Newly Created Eastmain-1 Reservoir in Northern Quebec, Canada, Ecosystems, 14, 28–46, doi:10.1007/s10021-010-9393-7, 2011.

Thornton, K. W.: Sedimentary processes, in: Reservoir Limnology: Ecological Perspectives, edited by: Thornton, K. W., Kimmel, B. L., and Payne, F. E., John Wiley & Sons, New York, 43–70, 1990.

Thorpe, S. A. and Jiang, R.: Estimating internal waves and diapycnal mixing from conventional mooring data in a lake, Limnol. Oceanogr., 43, 936–945, 1998.

Verburg, P. and Antenucci, J. P.: Persistent unstable atmospheric boundary layer enhances sensible and latent heat loss in a tropical great lake: Lake Tanganyika, J. Geophys. Res.-Atmos., 115, D11109, doi:10.1029/2009jd012839, 2010.

Vidal, J., Marce, R., Serra, T., Colomer, J., Rueda, F., and Casamitjana, X.: Localized algal blooms induced by river inflows in a canyon type reservoir, Aquat. Sci., 74, 315–327, doi:10.1007/s00027-011-0223-6, 2012.

Wan, Z.: New refinements and validation of the MODIS Land-Surface Temperature/Emissivity products, Remote Sens. Environ., 112, 59–74, doi:10.1016/j.rse.2006.06.026, 2008.

Wan, Z. and Dozier, J.: A generalized split-window algorithm for retrieving land-surface temperature from space, IEEE Trans. Geosci. Remote Sens., 34, 892–905, doi:10.1109/36.508406, 1996.

Wanninkhof, R.: Relationship between wind-speed and gas-exchange over the ocean, J. Geophys. Res.-Oceans, 97, 7373–7382, doi:10.1029/92jc00188, 1992.

Weiss, R. F.: Carbon dioxide in water and seawater: the solubility of a non-ideal gas, Mar. Chemi., 2, 203–215, 1974.

Wetzel, R. G. and Likens, G. E.: Limnological Analyses, Springer, New York, 429 pp., 2000.

Wüest, A. and Lorke, A.: Small-scale hydrodynamics in lakes, Annu. Rev. Fluid. Mech., 35, 373–412, doi:10.1146/annurev.fluid.35.101101.161220, 2003.

Zhao, Y., Wu, B. F., and Zeng, Y.: Spatial and temporal patterns of greenhouse gas emissions from Three Gorges Reservoir of China, Biogeosciences, 10, 1219–1230, doi:10.5194/bg-10-1219-2013, 2013.